Environ Sci Pollut Res
DOI 10.1007/s11356-014-2625-1

RESEARCH ARTICLE

Organic-coated nanoparticulate zero valent iron for remediation of chemical oxygen demand (COD) and dissolved metals from tropical landfill leachate

S. S. R. M. D. H. R. Wijesekara · B. F. A. Basnayake · Meththika Vithanage

Received: 7 August 2013 / Accepted: 4 February 2014

Abstract The use of nanoparticulate zero valent iron (NZVI) in the treatment of inorganic contaminants in landfill leachate and polluted plumes has been the subject of many studies, especially in temperate, developed countries. However, NZVI's potential for reduction of chemical oxygen demand (COD) and treatment of metal ion mixtures has not been explored in detail. We investigated the efficiency of NZVI synthesized in the presence of starch, mercaptoacetic, mercaptosuccinic, or mercaptopropenoic acid for the reduction of COD, nutrients, and metal ions from landfill leachate in tropical Sri Lanka. Synthesized NZVI were characterized with X-ray diffraction (XRD), transmission electron microscopy, X-ray photoelectron spectroscopy, scanning electron microscopy (SEM), thermal gravimetric analysis, Fourier transform infrared spectroscopy (FTIR) and Brunauer–Emmett–Teller. Of the samples tested, Starch-NZVI (S-NZVI) and mercaptoacetic-NZVI (MA-NZVI) performed well for treatment both COD and metal mixture. The removal percentages for COD, nitrate-nitrogen, and phosphate from S-NZVI were 50, 88, and 99 %, respectively. Heavy metal removal was higher in S-NZVI (>95 %) than others. MA-NZVI, its oxidation products, and functional groups of its coating showed the maximum removal amounts for both Cu (56.27 mg g^{-1}) and Zn (28.38 mg g^{-1}). All mercapto-NZVI showed well-stabilized nature under FTIR and XRD investigations. Therefore, we suggest mercapto acids as better agents to enhance the air stability for NZVI since chemically bonded thiol and carbonyl groups actively participation for stabilization process.

Keywords Nanoparticle · Zero valent iron · Fe(0) · Chemical oxygen demand · COD · Heavy metals · Mercaptoacetic acid · Starch

Introduction

Zero valent ion (ZVI), which can degrade a wide range of hazardous pollutants, is successfully used for environmental remediation, e.g., degradation of the chlorinated hydrocarbons in water (He and Zhao 2007). Comparative studies have shown that the nanoparticulate (<100 nm) zero valent iron (NZVI) degrade contaminants faster than micro-ZVI particles (Alidokht et al. 2011). The high reactivity of the NZVI is mainly related to large specific surface area, even though quantum size effects may also contribute to that (Li et al. 2006).

Several methods have been developed to synthesize ZVI particles, for example through laser-assisted formation, such as decomposition of iron penta carbonyl [$Fe(CO)_5$] in organic solvents or in argon (Elihn et al. 1999), thermal cracking of iron penta carbonyl (Karlsson et al. 2005), vacuum sputtering (Kuhn et al. 2002), reduction of goethite and hematite particles (Uegami et al. 2003), and most, commonly, reduction of ferric or ferrous salts with sodium borohydride (Li et al. 2006; Alidokht et al. 2011; Kanel et al. 2006, 2008). Some of these methods employ stabilizing materials such as carboxymethyl cellulose, starch, polyacrylic acid, cellulose acetate, noble metals, and oil emulsion. Even so, the NZVI prepared with the above-stated stabilizing materials tend to be either

Responsible editor: Angeles Blanco

Electronic supplementary material The online version of this article (doi:10.1007/s11356-014-2625-1) contains supplementary material, which is available to authorized users.

S. S. R. M. D. H. R. Wijesekara · M. Vithanage (✉)
Chemical and Environmental Systems Modeling Research Group, Institute of Fundamental Studies, Hanthana Road, Kandy 20000, Sri Lanka
e-mail: meththikavithanage@gmail.com

B. F. A. Basnayake
Department of Agricultural Engineering, University of Peradeniya, Peradeniya, Sri Lanka

Published online: 19 February 2014

aggregated or react fast with the surrounding media (Alidokht et al. 2011). Therefore, the synthesis of NZVI without oxidation by atmospheric oxygen remains a challenge. Mercapto acids have the potential to be a better stabilizing agent for NZVI because they have functional groups such as carboxylate and thiol that bind chemically to nanoparticles covering nanoparticulates surfaces avoiding its reactive reactions with atmospheric air (Bootharaju and Pradeep 2010; Chung and Lee 2004; Faccini et al. 2007). Furthermore, mercapto acids may counteract aggregation of other metallic nanoparticles (Tomonari et al. 2007; Chen and Kimura 2001), and possibly, they may have the same effect on NZVI, which would increase its injectability as well as its available surface area.

Consequently, NZVI is emerging as a new material for treatment of contaminated soil and groundwater that can be applied in situ and potentially replace the use of granular iron in reactive barriers. The treatment with NZVI has been extensively tested for heavy metal removal and degradation of pollution plumes, especially in temperate regions (Kanel et al. 2006; Blowes et al. 2000; Wang and Zhang 1997). For example, NZVI immobilize or degrade heavy metals like Cr^{6+}, As^{5+}, chlorinated hydrocarbons such as trichloroethene (TCE), pesticides (DDT, chlorpyrifos, lindane, etc.), and nutrients (nitrates, phosphates, etc.) (Li et al. 2006; Blowes et al. 2000; He and Zhao 2005; Hwang et al. 2011; Shea et al. 2004). Different approaches have been used to bring ZVI in contact with contamination. These include construction of permeable reactive barriers (PRBs), which contaminants flow into and in situ injection, where ZVI is delivered actively to the plume. The in situ injection of NZVI have shown significant efficiency with low operating costs compared to conventional ZVI PRBs (Li et al. 2006; Jun et al. 2009).

Landfill leachates from municipal solid waste (MSW) are variable and complex, reflecting the composition of solids deposited in the landfill. Many countries have identified leachate as a typical surface and ground water pollutant (Abdul et al. 2009; Christensen et al. 1998), especially in developing countries where open dumping occur without safety measures, such as landfill lining (Mor et al. 2006; Ariyawansha et al. 2009). MSW leachates often have high concentrations of heavy metals (such as Pb, Cd, Ni, Cr, Zn, Mn, Cu, and Fe), dissolved organic carbon components (such as humic, fulvic, and hydrophilic acids), inorganic ions (such as NO_3^-, NH_4^+, NO_2^-, PO_4^{3-}, SO_4^{2-}, Cl^-), and xenobiotic organic compounds (such as halogenated hydrocarbons, aromatic hydrocarbons, phenols, and chlorinated aliphatics) (Al-Wabel et al. 2011; Asadi 2008; Christensen et al. 1998; Kale et al. 2010). Chemical oxygen demand (COD) describes the organic matter content that is susceptible to oxidation by a strong chemical agent. This parameter reflects the changes of solid waste degradability in dumpsites and organic contaminant amount (Irene 1996). Most leachates from the early stages (first year) of landfill operation show high COD (above 20,000 mg L^{-1}). With time, the landfill material ages and COD stabilizes at values of 3,000 mg L^{-1} or less (Irene 1996). Excessive accumulation of these inorganic and organic pollutants can have detrimental effects on soil fertility, affect ecosystem function and constitute a health risk to animals and humans (Sun et al. 2001). Unfortunately, most of studies that have been conducted on landfill leachate treatment using NZVI are limited to application in temperate countries (Jun et al. 2009). However, leachate characteristics can differ between temperate and tropical countries because of climatic differences and chemical variation stemming from dissimilar consumer patterns (Trankler et al. 2005).

Hence, the objectives of this study were (1) to synthesize, characterize, and compare the stability of NZVI that had been exposed to starch and different mercapto acids; (2) to assess the removal ability of heavy metals in metal ion mixtures; and (3) to investigate the treatment ability of tropical landfill leachate with the mercapto-coated NZVI.

Experimental

Material

Synthesis and sample preparation were carried out at room temperature inside an anaerobic chamber with 2 % H_2 and 98 % N_2 atmosphere. The chamber was equipped with fan boxes bearing Pd pellets that catalyze the reaction between H_2 and traces of O_2 as well as desiccants for removing the produced water. All chemical reagents were analytical grade (from Sigma Aldrich). Prior to use, distilled, deionized water was purged with nitrogen gas for 15 min to remove dissolved O_2.

Preparation of zerovalent iron nanoparticles

In total, five different types of NZVI were synthesized. All NZVIs were synthesized by adding 100 ml of 0.5 M sodium borohydride solution (made from $NaBH_4$) drop-wise into a flask containing 100 mL of 0.14 M ferrous sulfate solution (made from $FeSO_4{\cdot}7H_2O$) to reduce Fe(II) (Alidokht et al. 2011). Synthesis was done under continuous stirring in inert environment. Borohydride addition was completed in ~2 h to control particle size (Alidokht et al. 2011). For the starch-bearing NZVI, 5 % (*w*/*w*) starch was added into the ferrous sulfate solution, whereas the mercapto acids were added just after the NZVI synthesis. The mercapto acids included (1) 40 mL of mercaptosuccinic acid [$HOOCCH(SH)CH_2COOH$; MS] solution, prepared by dissolving 448.9 mg of MS in 100 mL absolute ethanol under ice-cold conditions in room temperature (based on recipe from Bootharaju and Pradeep 2010); (2) 600 μL mercaptoacetic acid ($HSCH_2COOH$; MA); and (3) 500 μL of mercaptopropionic acid ($HSCH_2CH_2COOH$; MP).

An additional 10 mL sodium borohydride was added, and the mixture was stirred under a nitrogen gas flow to avoid dissolving oxygen for 15 min to complete the reaction. The precipitated NZVI slurries were transferred to the centrifuged tubes and sealed them with parafilm immediately inside the chamber. Then, the NZVI particles were separated by centrifugation (Beckman GP Centrifuge) at 442 RCF for 10 min, and washed by resuspending the material in absolute ethanol. This procedure was repeated three times. After the final centrifugation, particles were dried in a freeze dryer for approximately 45 min, and prepared particles were stored below 4 °C.

Characterization of NZVI

Samples characterized using X-ray diffraction (XRD), scanning electron microscopy and energy dispersive X-ray spectroscopy (SEM-EDX), transmission electron microscopy (TEM), Brunauer–Emmett–Teller (BET) surface area determination, and X-ray photoelectron spectroscopy (XPS). XRD was performed on a STOE Stadi-p transmission powder diffractometer with CuKα1 radiation at Copenhagen University. The scan range was from 0 to 70°(2θ) with a step size of 0.1° and 20 s measurement time per step. To avoid oxidation during the measurement, samples were soaked in glycerol before exit from the anaerobic chamber. TEM was carried out on a Phillips CM20 using an accelerating voltage of 200 kV. The TEM samples were resuspended in ethanol, deposited on Cu grids, and transported to the TEM inside a sealed container (5 min). SEM-EDX was performed on a FEI Quanta FEG SEM in low vacuum mode so that coating could be avoided. Samples were mounted on carbon tape on Al-sample holders and were transported (5 min) to the SEM in sealed containers. Specific surface area was determined with N_2 BET using a Quantachrome after degassing of samples at 100 °C for 24 h. Samples were prepared and mounted in sealed sample holders to avoid oxidation during transport and degassing. High-resolution XPS measurements were performed on Kratos Axis Ultra^{DLD} instrument fitted with a magnetic charge compensation system. The samples were transported out of the chamber, and a subsample was placed onto a piece of carbon tape on a stainless steel holder before being put into vacuum. All spectra were collected under high vacuum (9×10^{-9} to 4×10^{-8} torr) using an Al K-alpha source and about 500-μm spot size. Survey (broad scan) spectra were collected at 160 eV pass energy and all high-resolution scans (i.e., C 1 s) at 10 eV. Instrumental resolution is about 0.35 eV at 10 eV pass energy. Charge compensation was adjusted for each sample to obtain the narrowest line widths. All binding energies were referenced to adventitious C (285.0 eV). All spectra were recorded at room temperature (~30 °C). The XPS spectra were fitted using the Casa software.

Approximately 10 mg of sample was transferred to a platinum crucible inside an anaerobic chamber, and the thermal gravimetric analysis (TGA) was conducted from 25 to 500 °C at 10 °C min^{-1} heating rate in open atmosphere using a SCINCO STA N-650, a simultaneous thermal analyzer, equipped with a programmable temperature furnace. Fourier transform infrared spectroscopy (FTIR) was carried out on a Nicolet 6700 to probe the stability of dry NZVI particles in contact with air. Sample pellets were prepared for FTIR by mixing 10 mg NZVI with 100 mg of FTIR grade KBr. The transmission spectra were obtained from each pellet between 4,000 and 400 cm^{-1}, with 4 cm^{-1} resolution. The spectral analyses were performed with the software OMNIC (version 7.3).

Characterization of landfill leachate

The landfill leachate used in the experiment was collected from one of a main drainage stream point near the dumpsite in the Gohagoda open dumpsite, which is situated in the world heritage city Kandy, Sri Lanka (7° 18′ 47.85″ N and 80° 37′ 19.02″ E). The collected leachates were characterized for basic constitutes and properties such as pH, temperature, conductivity, alkalinity, total dissolved solids (TDSs), and dissolved oxygen (DO) in the field. Immediately thereafter, the samples were cooled to 4 °C and transferred to the laboratory for determination of chloride, metal, nutrient concentration, COD, and solids [total suspended solids (TSS), volatile suspended solids (VSSs), total solids (TS), volatile solids (VS), and settable solids] analysis. The leachate characterization methods and chemical constituents are shown in Table 1.

Batch experiments with landfill leachate

Batch experiments were carried out to determine the kinetics of NZVI reaction with leachate constitutes. One hundred milligrams (1 g L^{-1}) of NZVI was added to separate 100-mL portions of leachate outside the anaerobic chamber, and the containers were sealed. Leachate without NZVI was used as control samples. The resulting slurries were shaken at 100 rpm (EYELA B603 shaker), and samples were transferred to centrifuge tubes after 4, 12, 24, 72, and 120 h. After ultracentrifugation (RC26PLUS, SORVALL), the supernatant was decantered for determination of contaminant concentration.

Batch experiments with synthetic leachate

To simulate a "worst-case-scenario" with respect to heavy metal concentration, studies were conducted at room temperature with different initial metal concentrations using synthetic leachate with 1 g L^{-1} NZVI solutions purged with N_2 for 10 min to remove dissolved oxygen. Samples were kept for an additional 1 h to equilibrate the solution and solid in sealed containers to minimize oxidation.

The reactions were started by extracting 20 mL of the slurry per experiment and adding 10–500 μL synthetic leachate with

Table 1 Summary of the major chemical constituents of leachate from Gohagoda open landfill, Kandy

Constituents	Concentration[a]	Method	Reference
pH	8.29	ROSSsure-flow combination epoxy body electrode	
EC	14.13	Conductivity meter (Orion 5 star series)	
TDS	6,331		
BOD_5	270	Winkler method	APHA 2005
COD	6,355	Spectrophotometer (HACH DRB 200)	
TS	15,501	Membrane filter paper techniques	APHA 2005; Metcalf 1991
TSS	3,831		
VS	3664		
VSS	1,153		
Settable solids	1,972		
Alkalinity	3,236	Titrimetric method	Deutsch 1997
Hardness	2,241		APHA 2005
Ammonium–nitrogen	239	Iron-selective electrode	
Chloride	320		
Nitrate-nitrogen	172	Cadmium reduction method	
Nitrite-nitrogen	113	Diazotization method	
Phosphate	23	Ascorbic acid method	
Zinc	0.055	Atomic absorption spectrophotometer (GBC 933A, Australia)	
Cadmium	0.011		
Nickel	0.071		
Chromium	0.079		
Copper	0.174		
Lead	0.015		
Iron	1.496		
Manganese	0.324		
Aluminum	0.119		
Arsenic	0.002	Hydride generator atomic absorption spectroscopy	

[a] All in milligram per liter except pH and EC (mS/cm)

consisted of metal mixtures. This resulted in initial metal concentrations ranging from 5.0 to 250 mg L^{-1} for Zn(II) and Ni(II); 2.5 to 125 mg L^{-1} for Cu(II) and Pb(II); and 0.5 to 25 mg L^{-1} for Cr(III) and Cd(II). The pH was adjusted to 6.0 after addition of synthetic leachate using 0.1 M HNO_3 since it is reported that the acidic and neutral pH effective for adsorption of metal ions (Kanel et al. 2006). Then, the centrifuge tubes were then shaken at 100 rpm overnight. To separate solid and solution, the tubes were centrifuged at 6,842 RCF at room temperature, and the supernatant was transferred to a separate tube for metal analysis. The solid portion was dried in a nitrogen gas containing anaerobic chamber and characterized with FTIR, SEM-EDX, and XPS. Control experiments were performed in the absence of nanoparticles but with otherwise identical experimental conditions.

Effectiveness of organic coating of NZVI

To determine if the coating influenced reduction kinetics, experiments were performed with ~25 mg L^{-1} Cr(VI) (made from $K_2Cr_2O_7$) and 1 g L^{-1} NZVI prepared with the same procedure as the synthetic leachate experiment. The resulting slurries were shaken at 100 rpm (EYELA B603 shaker), and 10-mL samples were transferred to centrifuge tubes after 1, 4, 12, 24, and 72 h. In addition, a control experiment was performed in the absence of NZVI particulates. After ultracentrifugation, the supernatant was separated for determination of Cr(VI) by dipenyl carbazide method (Broadway et al. 2010).

Results and discussion

Characterization of synthesized NZVI

The XRD patterns of the synthesized NZVIs were similar and showed peaks consistent with metallic Fe (Fig. 1 for S-NZVI). In addition, a minor peak is observed at $2\theta \approx 20°$ and a broad peak at $2\theta \approx 35°$, suggesting the presence of minor amounts of goethite and ferrihydrite from oxidation. The BET surface area of the S-NZVI, MA-NZVI, MS-NZVI, and MP-NZVI

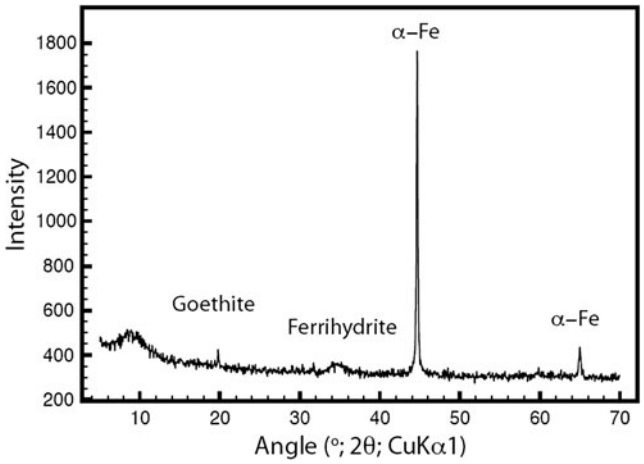

Fig 1 XRD pattern for synthesized starch (5 %) coated NZVI. The peaks are consistent with the presence of metallic iron, goethite, and ferrihydrite

particles yielded quite values of 136.0, 28.7, 144.0, and 24.9 $m^2\ g^{-1}$. The molecular weights of each coating agents differ from each other, and accordingly, the number of ligands such as hydroxyl, thiol, and carboxyl groups can be considered as starch>MSA>MPA=MAA. MPA and MAA are quite similar in thiol and carboxyl groups, and the only difference between them is the methyl groups. These ligands bond with resulted metallic iron clusters during the synthesis of NZVI. In this synthesis, the coating agent with highest number of ligands was involved to result more compacted or tiny nanoparticulates exhibiting high surface area. And the monocarboxylic acids with different methyl groups gave lowest surface area. MSA exhibited higher surface area than that of the starch coated NZVI. This may be due to the presence of two carboxylic functional groups in MSA, which may act as proton donar ligands in the synthesis process. High reactivity may have been responsible in binding many MSAs to a nanoparticle, which could increase its surface area. However, the resulted surface area might be affected by artifacts during drying, where the organic material and the NZVI could form aggregates, whose internal surfaces are isolated from N_2. TEM images of S-NZVI show 20–200 nm aggregates of NZVI particles covered with material that resemble curled up sheets, presumable the starch (Fig. 2).

The TGA from S-NZVI shows a loss of mass as a function of temperature (Fig. 3a). The weight loss of up to 40 °C is most likely caused by loss of ethanol from the washing procedure. This loss is visible as an endothermic peak in the differential thermal analysis (DTA) curves around 40 °C. The weight loss around 290 °C can be interpreted as a result of degradation of starch (Xu et al. 2004). Similarly, the exothermic reaction recorded in the DTA curve between 260 and 275 °C may be caused by the oxidation of C and H in starch to CO_2 and H_2O. Further, the exothermic sharp increments in the DTA curve around 425 °C suggest transformation of the maghemite to bulk to hematite (Ichiyanagi and Kimishima 2002). On the basis of the TGA, the weight loss by ethanol and starch thermal decomposition and remarkable weight increments by formation of oxidative compounds were observed.

FTIR was used to explore the coordination of the organic material to the NZVI as well as to probe the oxidation of the material when exposed to air. FTIR measurements of pure, uncoated NZVI show a well-defined IR peak at ~1,600 cm^{-1} for HOH (from water) and a board, undefined peak from 3,000 to 3,500 cm^{-1} from hydroxyl stretch (Fig. 4A: a). These characteristics are consistent with previous FTIR study (Lin et al. 2009) and indicates that the material is partially oxidized and trend to formation of goethite.

FTIR of the organic containing NZVI's show shift in peak position as well as new peaks (Fig. 4A: b–e). The peak at 3,000–3,500 cm^{-1} is more defined with a maximum at 3,390 cm^{-1}, and several peaks have appeared in the region 500–1,300 cm^{-1}. Some of these are attributable to the presence of Fe oxides from partial oxidation (Allabaksh et al. 2010). The peaks around 864 cm^{-1} can be attributed to the Fe–OH in plane and out of-plane bending vibrations, possibly due to the formation of Fe oxyhydroxide like goethite and maghemite (Online Resource 1) (Fang et al. 2012; Jayarathne et al. 2012). Compared to the pure NZVI, FTIR features additional peaks that are not related to the presence of Fe oxides (Allabaksh et al. 2010):

The band at ~625 cm^{-1} might be cause by antisymetric bend of sulfate that was not removed during the rinsing (Knittle et al. 2001). Similarly, the absorption at ~1,300–1,000 cm^{-1} is consistent with strong stretching vibrations of C–O, suggesting remaining ethanol after washing procedure (Stuart 1996).

2) Absorption in the region 1,550–1,650 cm^{-1} can be assigned to carboxylate groups in the material (Hernandez et al. 2005). Previous studies show that the COO–H and O–H stretch (around 3,030 cm^{-1}), S–H stretch (around 2,600–2,540 cm^{-1}), and C=O strong stretch modes (around 1,720 cm^{-1}) disappeared after mercapto acids coating procedures to the Ag surfaces (Chung and Lee 2004; Pretsch et al. 1989). In agreement, these peaks were not observed in this study. The lack of a bands representing carbonyl (around 1,720 cm^{-1}) and thiol (around 2,600 cm^{-1}) groups suggests that a monolayer of mercapto acid is adsorbed mainly via both thiol and carboxylate on to the metallic Fe. For metallic Ag, mercaptoacetic acid coordinated preferentially through the thiol group, exposing uncomplexed carboxylic acid groups (Lee et al. 2000). Hence, it could be a competitive adsorption of thiol and carboxylate groups on Fe-oxide layer surfaces and the head group-metal interaction could be played a key role determining the adsorption behavior.

Based on the FTIR results, postulated mechanisms for NZVI coatings are shown in Fig. 5. Figure 5a–c shows the mercaptoacetic, mercaptosuccinic, and mercaptopropionic

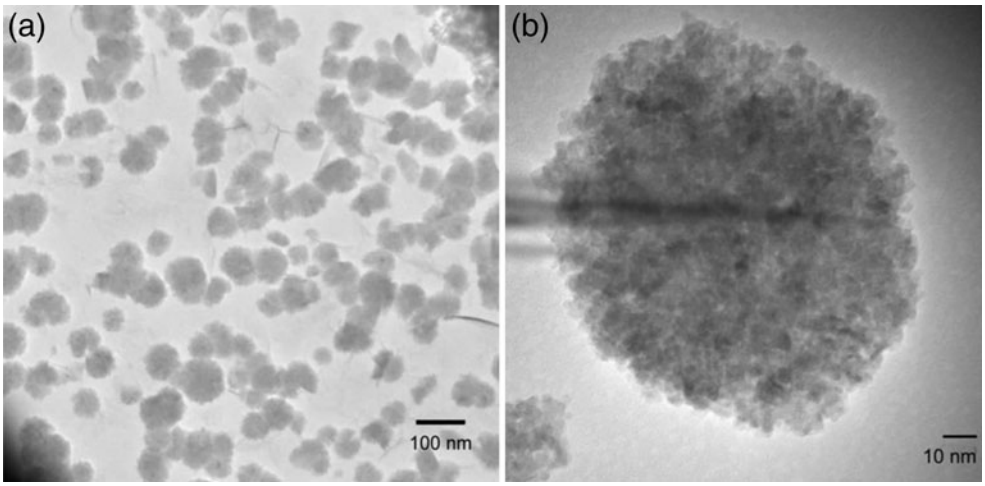

Fig. 2 **a** The TEM images of aggregates of starch (5 %) coated NZVI. The scale bar represents 100 nm in **a** and 10 nm in **b**

acid adsorbing on Fe-oxide layer surfaces via carboxylate and thiol groups.

Figure 3b shows FTIR of S-NZVI as a function of time when it is exposed to the atmosphere. No peak changes are noticeable during the 5-h experiment suggesting that S-NZVI is protected from oxidation by atmospheric O_2 by the starch. FTIR measurements performed on material that had been exposed for 48 h (Online Resource 2 and 3) shows oxidation of the sample in the atmosphere. Compared to coated NZVI spectrums, more defined board peak at 3,390 cm^{-1} wavenumbers was observed in the air exposed pure NZVI, and its interaction with water molecules suggests it is nonstable nature in the open atmosphere even after 48 h of synthesis. Hence, FTIR data indicate that mercapto acids increase the NZVI stability. Except MP-NZVI, all other synthesized NZVI were stable in air for about a period of 21 days based on the color observations. However, the material became unstable after 3 weeks of aging, resulting in rapid oxidation when exposed to air.

Reactions of NZVI with aqueous ions

Cr(VI) reduction capability

Experiments with chromate and pure and organic containing NZVI were conducted to determine if redox reactions with dissolved compounds were hampered by the presence of organic material. In addition, these experiment were used to understand the effect of the organic coating on the Cr(VI) removal. The $CrO_4^{2-}/Cr(OH)_3$ standard electrode potential is −0.13 V compared to −0.41 V for Fe2+/Fe(0) (Krauskopf and Bird 1995), and it is readily reduced by Fe(0) (Xu and Zhao 2007). In its hexavalent state, chromium is soluble as chromate species, but upon reduction, it becomes much less

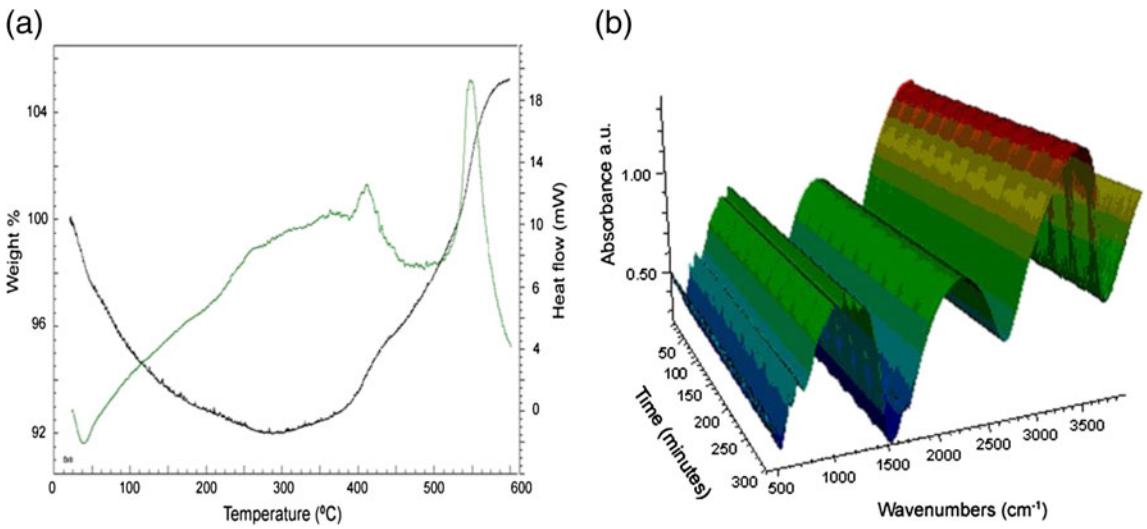

Fig. 3 **a** DTA and TGA curve of starch-coated NZVI under air in the temperature range between room temperature to 600 °C at 10 °C min^{-1} heating rate. *Green and black lines* are for DTA and TGA respectively (**b**). Time scanning FTIR spectrum of starch coated NZVI obtained in transmission mode between 4,000 and 400 cm^{-1}, with 4 cm^{-1} resolution

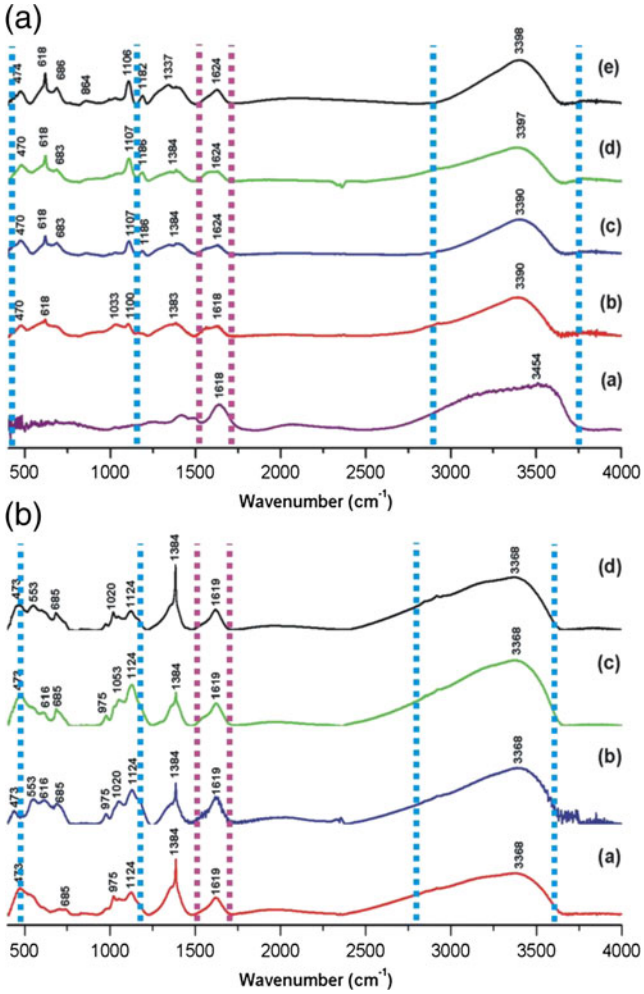

Fig. 4 **A** Transmission FTIR spectra of *a* non-stabilised nano zero valent iron, *b*mercaptoacetic, *c* mercaptopropionic, *d* mercaptosuccinic acids, and *e* starch-coated nanozero valent irons. **B** Metal-treated nanozero valent iron residue spectra of *a* mercaptoacetic, *b* mercaptopropionic, *c* mercaptosuccinic acids, and *d* starch coated nanozero valent iron are taken in transmission mode

soluble and precipitates as Cr(III)-bearing (oxyhydr)oxides. In our experiments, we would expect reactions such as:

$$Fe^{o}_{(s)} + CrO_4^{2-}{}_{(aq)} + 4H_2O_{(l)} \rightarrow Cr(OH)_{3(s)} + Fe(OH)_{3(s)} + 2OH^{-}{}_{(aq)} \quad (1)$$

Experiments with both pure and organic-containing NZVI showed rapid removal of Cr(VI) with rates that were very similar (Online Resource 4). This indicates that the organic compounds do not interfere greatly with its redox reaction and the removal amount.

Effect of NZVI on leachate

Chemical oxygen demand removal by NZVI A range of biodegradable (sugars, starch, cellulose, fat, protein, etc.), non-biodegradable (aromatic hydrocarbon, aliphatic compounds, etc.) and humic substances (humic, hydrophilic, fulvic acid, etc.) are found in landfill leachates (Jun et al. 2009; Lai et al. 2007) and contribute to the COD. In the experiments, the initial COD was ~6,000 mg L^{-1} and decreased during the studied 72 h (Fig. 6a). COD removal was very similar for the organic-containing NZVI with a maximum removal of 56 % for MP-NZVI and minimum of 50 % for S-NZVI. The COD may decrease as a result of organic compound adsorption and coprecipitation with iron corrosion products (Wang et al. 2010).

Phosphate (PO_4^{3-}) removal by NZVI Phosphate removal was observed as a function of reaction time. For S-NZVI, almost complete removal (~80 %), of phosphate occurred within the first 4 h. After 72 h, MA-, MS-, and MP-NZVI had also caused significant phosphate removal (>80 %). The initial concentration of phosphate decreased from 1.741×10^{-4} mol L^{-1} to 3.405×10^{-5} mol L^{-1} indicating with ~80 % removal percentage showing 1.029×10^{-6} mol m^{-2} removal density by S-NZVI within 4 h. The maximum phosphate removal of 99 % was indicated by S-NZVI with a removal density of 1.269×10^{-6} mol m^{-2} after 72 h. For the MS-NZVI, initial phosphate removal up to 75 % showed 9.171×10^{-7} mol m^{-2} after 12 h, and it was then continued to remove, indicating 87 % removal with a 1.050×10^{-6} mol m^{-2} removal density after 24 h (Fig. 6b). However, due to high pH in the media, weakly bound phosphate groups can be desorbed (Almeelbi and Bezbaruah 2012). In addition, the presence of natural organic matter (NOM) and nitrate may possess effects on phosphate removal by NZVI (Almeelbi and Bezbaruah 2012). In addition, NZVI tends to cause rapid corrosion in aqueous media depleting dissolved oxygen creating anoxic environment and high pH (Almeelbi and Bezbaruah 2012). Phosphate ions may adsorb on the corroded NZVI (e.g. goethite). This may be a reason for increment of phosphate removal through biological phosphate removal processes since the anoxic environment is favorable for microorganisms (*Microlunatus phosphovorus*, *Lampropedia* spp., etc.) activity, which contributed to degrade phosphate (Mino et al. 1998).

Nitrate nitrogen (NO_3^-–N) and nitrite nitrogen (NO_2^-–N) removal by NZVI Nitrogen-based compounds are also a major constituent in landfill leachate and cause serious environmental issues. They exist as ammonium, ammonia, nitrate, and nitrites, which are the main by-products of protein and urea degradation (Jun et al. 2009). The removal densities of nitrate–nitrogen and nitrite–nitrogen with time are shown in Fig. 6c and d. The initial concentration of nitrate–nitrogen and nitrite–nitrogen was 6.68×10^{-3} mol L^{-1} and 1.40×10^{-3} mol L^{-1}, respectively. Tested NZVI showed nitrate–nitrogen removal densities as 4.433×10^{-5}, 1.600×10^{-4}, 4.060×10^{-5}, and 1.900×10^{-4} mol m^{-2} for S, MA, MS, and MP-NZVI, respectively, within 72 h of reaction period. These

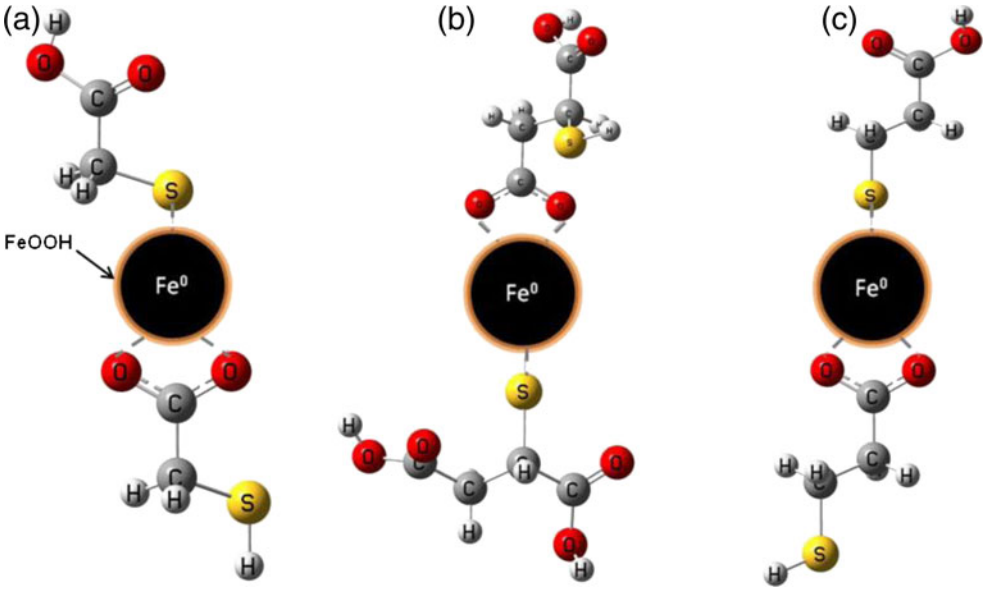

Fig. 5 Schematic representations for the adsorption of monolayer's of **a** mercaptoacetic acid, **b** mercaptosuccinic acid, and **c** mercaptopropionic acid coated with nanozero valent iron surfaces via carboxylate and thiol functional groups

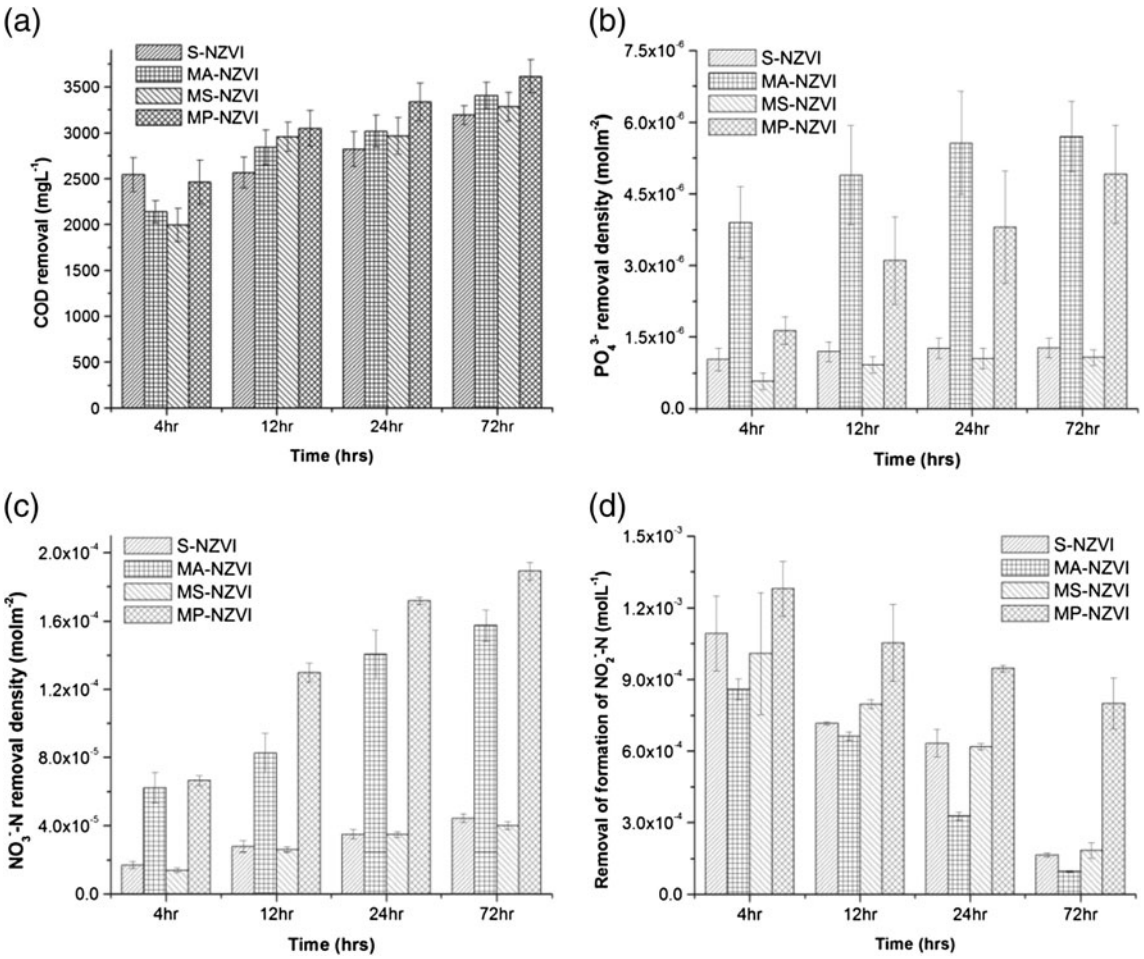

Fig. 6 Batch experiment results for **a** chemical oxygen demand (COD), **b** phosphate (PO_4^{3-}), **c** nitrate nitrogen (NO_3^-–N) and **d** nitrite nitrogen (NO_2^-–N) while reacting leachate with starch, mercaptoacetic, mercaptosuccinic, and mercaptopropionic acid coated nanozero valent iron solutions (1 g L^{-1}). Error bars represents: average±SDs

results were agree with previous batch experiments for nitrate removal studies (Hwang et al. 2011).

The nitrite–nitrogen behavior was observed following similar pattern observed for nitrate nitrogen removal (Fig. 6d). The S, MA, and MS-NZVI indicated removal of nitrite–nitrogen 88, 93, and 86 %, respectively, after 72 h reaction period. However, MP-NZVI showed ~40 % nitrite–nitrogen removal after 72 h indicating lowest removal.

The concentration of nitrogen species is mainly related to oxidation–reduction reactions. Anaerobic ammonium oxidation (anammox), denitrification, and sorption processes may occur. NZVI may release electrons during the dehalogenation process that could dissociate water molecules to hydrogen and hydroxyl ions, and they can be involved in nitrate reduction produces ammonium and ferrous ions (reaction 2) (Hsu et al. 2011). The reduction of nitrate could also occur via other pathways, producing nitrite and nitrogen gas. The reactions involved are shown in reaction 2, 3, 4, and 5 (Hsu et al. 2011).

$$4Fe^{0}{}_{(s)} + NO_{3\,(aq)}^{-} + 10H^{+}{}_{(aq)} \rightarrow 4Fe^{2+}{}_{(aq)} + NH_{4\,(aq)}^{+} + 3H_2O_{(l)} \quad (2)$$

$$5Fe^{0}{}_{(s)} + 2NO_{3\,(aq)}^{-} + 12H^{+}{}_{(aq)} \rightarrow 5Fe^{2+}{}_{(aq)} + N_{2(g)} + 6H_2O_{(l)} \quad (3)$$

$$Fe^{0}{}_{(s)} + NO_{3\,(aq)}^{-} + 2H^{+}{}_{(aq)} \rightarrow Fe^{2+}{}_{(aq)} + NO_{2\,(aq)}^{-} + H_2O_{(l)} \quad (4)$$

$$2Fe^{0}{}_{(s)} + 2H_2O_{(l)} + O_{2(aq)} \rightarrow 2Fe^{2+}{}_{(aq)} + 4OH^{-}{}_{(aq)} \quad (5)$$

$$Fe^{0}{}_{(s)} + 2H_2O_{(l)} \rightarrow Fe^{2+}{}_{(aq)} + H_{2(g)} + 2OH^{-}{}_{(aq)} \quad (6)$$

Depending on the reaction product, 1–5 mol of NZVI are required to reduce 1 mol of nitrate. Reactions 4 and 5 require highly acidic media, which is unlikely in leachate media. The ammonium concentrations should also be considered for a better understanding of the process. Under anoxic conditions, ammonium can be converted to nitrogen gas with nitrite as the electron acceptor (Jun et al. 2009).

Effect on heavy metal removal by NZVI in actual leachate The NZVI had high removal efficiencies for all heavy metal in the leachate, indicating <5 % of the initial concentration was presented after analysis. The removal of the heavy metal from solution could occur through several mechanisms such as reduction, adsorption, and precipitation. The pH of the media plays a major role in here. For instance, the medium pH increases by the production of OH^- (Eqs. 5 and 6) favoring for metal hydroxide precipitation:

$$Me^{n+}{}_{(aq)} + OH^{-}{}_{(aq)} \rightarrow Me(OH)_{n\,(S)} \quad (7)$$

where Me^{n+} denotes a metal with charge $n+$ and $Me(OH)_{n(S)}$ its solid hydroxide.

In addition to precipitation, high pH will favor adsorption of metals to the Fe-oxide corrosion products through surface complexation:

$$\equiv FeOH + Me^{n+}{}_{(aq)} + OH^{-}{}_{(aq)} \leftrightarrow \equiv FeOMe^{(n+-1)} + H_2O \quad (8)$$

where ≡FeOH denotes a surface hydroxyl adsorption site and $\equiv FeOMe^{(n+-1)}$, a metal surface complex.

Finally, some heavy metal ions can be reduced to their metallic state when reacting with metallic iron (reaction 9).

$$3Cu^{2+}{}_{(aq)} + 2Fe^{0}{}_{(s)} \rightarrow 2Fe^{3+}{}_{(aq)} + 3Cu_{(s)} \quad (9)$$

Further, it has been reported that sulfide ions present in the leachate (from the activity of sulfate reducing bacteria in the anoxic medium) and carbonate ions (tested alkalinity of leachate indicates a very high value) help to precipitate heavy metals (Jun et al. 2009).

To determine what reactions are thermodynamically favorable, aqueous speciation and saturation index (logarithm based) were calculated with PHREEQC (Parkhurst and Appelo 1999) and the MINTEQ (Allison et al. 1990) database using the database from Lawrence Livermore National Laboratory. The saturation index is defined as:

$$SI = \mathrm{Log}\,(IAP/Ksp),$$

where IAP is the ion activity product (i.e., the actual concentrations), and Ksp is the solubility product. For metals, the Ksp is defined based on the electron "concentration", i.e., the pe, which is equivalent to the Eh:

$$Ni(0) \gg Ni^{2+} + 2e- \quad K = 10^{8.112}$$

In addition, equilibrum constants for the reactions $Fe(0) \leftrightarrow Fe^{2+}+2e-$ ($K=10^{13.858}$) and $Ni(0) \leftrightarrow Ni^{2+}+2e-$ ($K=10^{8.112}$) were calculated from the metal's standard redox potentials (−0.41 V for Fe; −0.24 V for Ni; Krauskopf and Bird 1995). In the calculations, solutions are assumed to be in equilibrium with Fe(0) and atmospheric CO_2. Calculations for the synthetic leachates are based on the maximum concentrations used in the experiments and a pH of 6.5. Valencies for metals in the sampled leachate are estimated. The calculations show that reduction of Cu(II), Pb(II), and Ni(II) is thermodynamically possible, whereas reduction of Cd(II), Cr(III), and Zn(II) is not (Table 2). It also shows that of the nonmetallic phases present in the database only rhodochrosite, siderite, and $Fe(OH)_{2(S)}$ are supersaturated. Thus, the metal removal from solution largely stem from reduction and adsorption. Further, the calculations indicate PbOHCl (laurionite) is supersaturated in the experiments. If this phase precipitates, PHREEQC calculations indicate that it could account for around 80 % of the

Table 2 Thermodynamic calculations of saturation index (logarithm based) in experiments with synthetic leachate using PHREEQC (Parkhurst and Appelo 1999) and the MINTEQ database (Allison et al. 1990). In addition, equilibrum constants for the reactions $Fe(0) \leftrightarrow Fe^{2+} + 2e^-$ ($K = 10^{13.858}$) and $Ni(0) \leftrightarrow Ni^{2+} + 2e^-$ ($K = 10^{8.112}$) were calculated from the metal's standard redox potentials (−0.41 V for Fe; -0.24 V for Ni (Krauskopf and Bird 1995)). In the calculations, solutions are assumed to be in equilibrium with Fe(0) and atmospheric CO_2. Calculations for the synthetic leachates are based on the maximum concentrations used in the experiments and a pH of 6.5. Valencies for metals in the sampled leachate are estimated

Element and initial valency	Me(0)	Me hydroxide*	Me hydroxy-chloride*	$MeCO_{3(s)}$
Cd(II)	−3.4	−5.9	−3	−0.2
Cr(III)	−23	3.6		
Cu(II)	9.3			−13
Fe(0)	0			0.4
Ni(II)	4.2	−0.8		−4.8
Pb(II)	6.6	0.4	0.7	0.1
Zn(II)	−13.5	−1.6		−1.8

*Value for $Me(II)(OH)_2$, except for $Cr(III)(OH)_3$

elements removal in the experiments as PbOHCl precipitation with the highest Pb concentration.

Heavy metal removal by NZVI in synthetic leachate

According to the heavy metal removal experiments, maximum removal amounts were recorded for MA-NZVI indicating 56.27 and 28.38 mg g^{-1} for Cu(II) and Zn(II), respectively, at the initial concentrations as 119.53 mg L^{-1} [for Cu(II)] and 66.66 mg L^{-1} [for Zn(II)]. The Pb(II) and Ni(II) treated with MP-NZVI indicated 117.11 and 34.38 mg g^{-1} respectively becoming the highest removal amounts among the tested NZVIs at initial concentrations of 128.26 and 239.59 mg L^{-1} for Pb(II) and Ni(II), respectively. In addition, MS-NZVI showed around 65.53, 28.26, 23.64, and 22.12 mg g^{-1} becoming lowest removal amounts for Pb(II), Cu(II), Ni(II), and Zn(II), respectively, at initial concentrations as 72.66 [Pb(II)], 34.04 [Cu(II)], 207.63 [Ni(II)], and 121.20 [Zn(II)]mg L^{-1}. Results indicated only a slight difference among the removal amounts for tested nanomaterials (Online Resource 5). Adsorption, reduction, and precipitation processes may be the mechanisms for removal of heavy metal ions from the synthetic leachate (Alidokht et al. 2011; Jun et al. 2009).

Analyzing of standard reduction potentials, more negative reduction potential of lead as $Pb^{2+}+2e \longrightarrow Pb$ (−0.126 V) and more positive reduction potential of copper as $Cu^{2+}+2e \rightarrow Cu$ (+0.340 V) can be observed. Nickel (Ni^{2+}/Ni) and zinc (Zn^{2+}/Zn) have reduction potentials of (−0.25 V) and (−0.76 V), respectively. The reduction potential of iron as $Fe^{3+}+3e \rightarrow Fe$ (−0.030 V), hence $Fe \rightarrow Fe^{3+}+3e$ (0.030 V). Hence, the emf for the reactions were Zn^{2+}/Fe, Ni^{2+}/Fe, Pb^{2+}/Fe, and Cu^{2+}/Fe as −0.79, −0.28, −0.156, and 0.31 V, respectively. The Gibbs free energy change (ΔG) is negative for thermodynamically feasibly reactions and if emf positive or emf>0, ΔG becomes negative or $\Delta G<0$ (Peter 2001). Similarly, ΔG for Zn^{2+}/Fe, Ni^{2+}/Fe, Pb^{2+}/Fe, and Cu^{2+}/Fe systems can be calculated as ΔG Cu<<0<Pb<Ni<<Zn. Therefore, reduction of Cu(II) is feasible than Pb(II) by metallic iron. In that case, MA-NZVI showed Pb(II) uptake than Cu(II) (Online Resource 5). Possibly, this may be due to complexation reactions of divalent metals in to mercato acids and the PbOHCl precipitation (Devipriya et al. 2013; Bootharaju and Pradeep 2010).

SEM and EDX analyses

SEM images were taken for MP-NZVI after it was reacted with the synthetic leachate show large aggregates of particles (~350 nm) (figure is not shown). EDX spectra (Online Resource 6) and maps were collected, to confirm the composition of the material. The elemental maps show that the material is homogeneous on a micrometer scale as expected, and consists mostly of Fe and O. Relative high amounts of Na, S, Zn, Cu, Ni, and Cr scavenged from the leachate were also observed.

XPS results

Figure 7a shows the XPS wide scan of reacted MP-NZVI. The peaks indicate the surface of the nanoparticles is mostly carbon (67.8 at.%) and oxygen (25.7 at.%). Iron (2.0 at.%), silicon (4.1 at.%), zinc (0.2 at.%), and lead (0.2 at.%) were also detected. High-resolution scans of the C 1s region give insight into why the C signal is so high (Fig. 7b). Most of the carbon contribution stems from C–C(H) bonds (285 eV). Usually, this contribution is associated with adventitious carbon, but some of it may also come from C–C(H) bonds in the mercaptopropionic acids. The C–O(H) (286.3 eV) and O=C–O bonds (288.8 eV), also stem from the mercaptopropionic acids. The observed Pb and Zn peaks indicate that the MP-NZVI is successful at immobilizing these elements.

With respect to iron, Li and Zhang (2007)explain that NZVI particles typically have a layered structure, with the inner core being zero-valent iron (Fe^0) and the outer shell as the iron oxides/hydroxides formed from oxidation. If zero-valent iron were present, a contribution at 706 eV would be expected in high resolution Fe 2p scans (Li and Zhang 2007; McIntrye and Zetaruk 1977). In this study, when looking at the Fe 2p region (Fig. 7c), no contribution at 706 eV is seen, so either the oxidised coating is too thick for the photoelectrons from the inner core to escape, or the zero-valent core has been completely oxidized. On average, only photoelectrons from the top 10 nanometers reach the detector and the operating conditions in this study (Nesbitt et al. 2004), so if the oxidized coating plus the coating from the acid were more than 10 nm

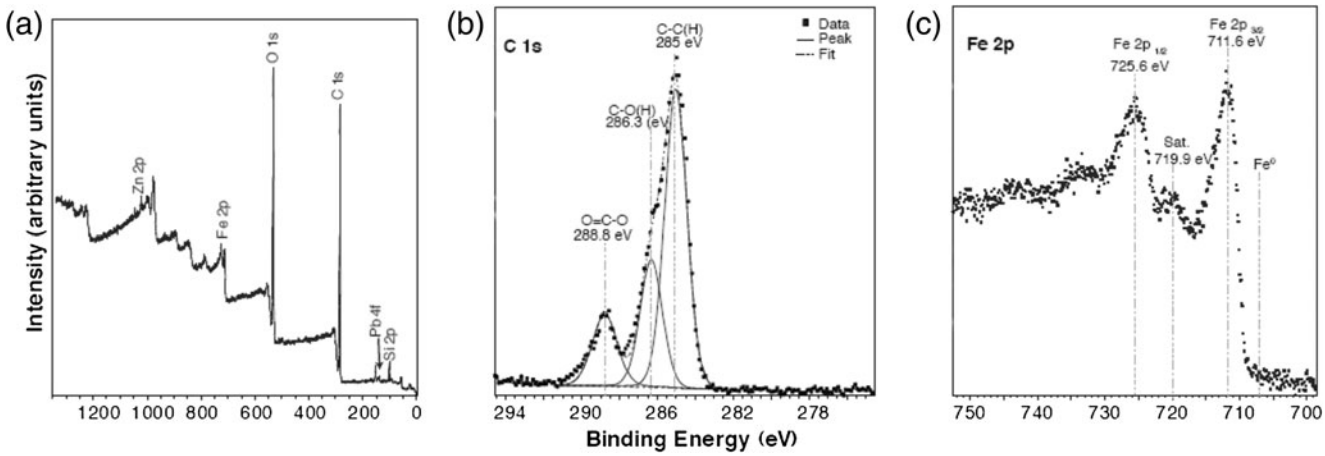

Fig. 7 **a** XPS wide-scan survey of reacted MP-NZVI. The major core levels are labeled. Unlabeled peaks are lesser lines of labeled peaks. **b** XPS high-resolution scan of the C 1s region on reacted MP-NZVI. The data (*squares*) have been fitted with peaks (*solid lines*) representing C–C(H) (285 eV), C–O(H) (286.3 eV), and O=C–O (288.8 eV) contributions. The fit of these peaks to the data is shown (*dotted line*) and **c** XPS high-resolution scan of the Fe 2p region of reacted MP-NZVI. The peaks for the Fe 2p spin-orbit split, the satellite (*sat.*) and zero valent iron contributions are indicated

thick, no contribution from the core of the nanoparticle would be detected. The peaks at 711.6 and 725.6 eV may correspond to the 2p 3/2 and 2p 1/2 contribution of oxidized Fe(III), respectively (Li and Zhang 2007; Baykal et al. 2012; McIntrye and Zetaruk 1977). However, similar peaks are identified as coming from FeO contributions (Cirtiu et al. 2011; Sun et al. 2006). After fitting peaks to the Fe 2p spectra, based on a comprehensive study by Biesinger et al. (2011) (Biesinger et al. 2011), we assign the 711.6 and 725.6 eV peaks to spin-orbit splitting of Fe in Fe(III) coordination. The peak at 719.9 eV is unanimously agreed upon as being the satellite Fe 2p contribution (Li and Zhang 2007; Baykal et al. 2012; Cirtiu et al. 2011; McIntrye and Zetaruk 1977; Mullet et al. 2008; Sun et al. 2006).

FTIR characteristics of residue after removal of heavy metals from synthetic leachate

FTIR measurements on NZVI's after they had reacted with the synthetic leachate (Fig. 4B) show important differences in the IR spectra. Compared with the nonreacted samples, the peak in the 3,300 cm^{-1} region appears broader due to the formation of Fe oxides. Further, the characteristic changes (1) peak at 1,380 cm^{-1} is much stronger, (2) appearance of a new peak at 1,124 cm^{-1}, and (3) significant changes at peak area between 710 and 570 cm^{-1} can be identified possibly due to sorption of metal ions on to NZVI and its oxidation products after the metal treatment.

Conclusions

In this study, we treated NZVI with starch and mercapto-based acids to stabilize them. The organic containing NZVI's were characterized and then reacted with landfill leachates to examine how NZVI's, synthesized in the presence of different organic compounds, removed organic, nutrients, and heavy metals. The time-resolved FTIR results indicate that mercapto acids and starch result in decreased reaction of NZVI with atmospheric O_2 in dry state. Further, FTIR measurements indicate that acids bond to the iron via carboxyl and thiol groups. Results from batch experiments demonstrated that synthesized NZVI could be used to remove organic contaminants from landfill leachates. The S-NZVI showed the highest removal efficiency for nitrate–nitrogen (88 %) and phosphate (99 %). However, the COD removal was observed as the lowest in the S-NZVI (50 %), and maximum removal of COD was recorded for MP-NZVI (56 %). Further, metal ion removal studies indicated that the maximum removal amounts for Cu (56.27 mg g^{-1}) and Zn (28.38 mg g^{-1}) for MA-NZVI. Comparing with other stabilizing NZVI in the literature, the mercaptoacids used stabilised materials well exhibited advanced characteristics features, for instance, high average BET surface area and high reactivity with high air stability. In addition, heavy metal removal efficiencies were recorded to be high for mercaptoacid-stabilized NZVI, comparing with other similar study with landfill leachate and synthetic metal mixtures. In summary, stabilized NZVI can be effectively used to treat tropical landfill leachates.

Acknowledgement The authors are most gratefully acknowledged Professor Knud Dideriksen, the Nano-Science Center, University of Copenhagen for sharing his expertise in nanotechnology. The authors are grateful to Professor Susan Stipp and Assistant Professor K.N. Dalby from University of Copenhagen for their support given for the XPS analysis. We would like to thank Fahmida Khurram from University of Copenhagen for XRD analysis. We thank M. Kulathunga and A. Herath, Dr. K. Mahatantila, Anushka, and Lakmal at the Institute of Fundamental Studies, Sri Lanka for their support given.

References

Abdul J, Vigneswaran S, Shon H, Nathaporn A, Kandasamy J (2009) Comparison of granular activated carbon bio-sorption and advanced oxidation processes in the treatment of leachate effluent. Korean J Chem Eng 26(3):724–730. doi:10.1007/s11814-009-0121-y

Alidokht L, Khataee AR, Reyhanitabar A, Oustan S (2011) Reductive removal of Cr(VI) by starch-stabilized Fe0 nanoparticles in aqueous solution. Desalination 270(1–3):105–110. doi:10.1016/j.desal.2010.11.028

Allabaksh MB, Mandal BK, Kesarla MK, Kumar KS, Reddy PS (2010) Preparation of stable zero valent iron nanoparticles using different chelating agents. J Chem Pharm Res 2(5):67–74

Allison JD, Brown DS, and Novo-Gradac KJ (1990) MINTEQA2/PRODEFA2—a geochemical assessment model for environmental systems: Version 30 User's Manual US Environmental Protection Agency Athens, GA

Almeelbi T, Bezbaruah A (2012) Aqueous phosphate removal using nanoscale zero-valent iron. J Nanopart Res 14(900):1–14. doi:10.1007/s11051-012-0900-y

Al-Wabel MI, Al Yehya WS, AL-Farraj AS, El-Maghraby SE (2011) Characteristics of landfill leachates and bio-solids of municipal solid waste (MSW) in Riyadh City, Saudi Arabia. J Saudi Soc Agric Sci 10:65–70. doi:10.1016/j.jssas.2011.03.009

American public health association (2005) Standard methods for the examination of water and wastewater. 21st ed, Washington

Ariyawansha RTK, Basnayake BFA, Pathirana KPMN, Chandrasena ASH (2009) Open dump simulation for estimation of pollution levels in wet tropical climates. 21st Annual congress, Postgraduate Institute of Agriculture, University of Peradeniya

Asadi M (2008) Investigation of heavy metals concentration in landfill leachate and reduction by different coagulants. The 7th International Conference on Environmental Engineering Faculty of Environmental Engineering, Vilnius Gediminas Technical University

Baykal A, Toprak MS, Durmus Z, Senel M, Sozeri H, Demir A (2012) Sythesis and characterisation of dendrimer-encapsulated iron and iron-oxide nanoparticles. J Supercond Nov Magn 25:1541–1549

Biesinger MC, Payne BP, Grosvenor AP, Lau LWM, Gerson AR, Smart RSC (2011) Resolving surface chemical states in XPS analysis of first row transition metals, oxides and hyrdoxides: Cr, Mn, Fe, Co and Ni. Appl Surf Sci 257:2717–2730

Blowes DW, Patacek CJ, Benner SG, McRae CWT, Bennett TA, Puls RW (2000) Treatment of inorganic contaminants using permeable reactive barriers. J Contam Hydrol 45:123–137

Bootharaju MS, Pradeep T (2010) Uptake of toxic metal ions from water by naked and monolayer protected silver nanoparticles: an X-ray photoelectron spectroscopic investigation. J Phys Chem C 114:8328–8336

Broadway A, Cave MR, Wragg J, Fordyce FM, Bewley RJF, Graham MC, Ngwenya BT, Farmer JG (2010) Determination of the bioaccessibility of chromium in Glasgow soil and the implications for human health risk assessment. Sci Total Environ 409:267–277

Chen S, Kimura K (2001) Synthesis of thiolate-stabilized platinum nanoparticles in protolytic solvents as isolable colloids. J Phys Chem B 105:5397–5403

Christensen JB, Jensen DL, Gron C, Filip Z, Christensen TH (1998) Characterization of the dissolved organic carbon in landfill leachate-polluted groundwater. War Res 32(1):125–135

Chung C, Lee M (2004) Self-assembled monolayers of mercaptoacetic acid on Ag powder: characterization by FT-IR diffuse reflection spectroscopy. Bull Korean Chem Soc 25(10):1461–1462

Cirtiu CM, Raychoudhury T, Ghoshal S, Moores A (2011) Systematic comparison of the size, surface characteristics and colloidal stability of zero valent iron nanoparticles pre- and post-grafter with common polymers. Colloids Surf A 390:95–104

Deutsch WJ (1997) Groundwater geochemistry fundamentals and applications to contamination. LEWIS Publishers, Boca Raton

Devipriya S, Arunadevi N, Vairam S (2013) Synthesis and thermal characterization of lanthanide(III) complexes with mercaptosuccinic acid and hydrazine as ligands. J Chem 2013:10. doi:10.1155/2013/497956

Elihn K, Otten F, Fornan M, Kruis FE, Fissan H, Carlsson JO (1999) Nanoparticle formation by laser-assisted photolysis of ferrocene. Nanostruct Mater 12:79–82

Faccini F, Fcbrric H, Schubert U, Wendel E, Tsetsgee O, Mu¨ller K, Bertagnolli H, Venzo A, Gross S (2007) -Mercapto-functionalized hafnium- and zirconium-oxoclusters as nanosized building blocks for inorganic–organic hybrid materials: synthesis, characterization and photothiol-ene polymerization. J Mater Chem 17:3297–3307. doi:10.1039/b702714a

Fang L, Cao Y, Huang Q, Walker SL, Cai P (2012) Reactions between bacterial exopolymers and goethite: a combined macroscopic and spectroscopic investigation. War Res 46:5613–5620

He F, Zhao D (2005) Preparation and characterization a new class of starch-stabilized bimetallic nanoparticles for degradation of chlorinated hydrocarbons in water. Environ Sci Technol 39:3314–3320

He F, Zhao D (2007) Manipulating the size and dispersibility of zerovalent iron nanoparticles by use of carboxymethyl cellulose stabilizers. Environ Sci Technol 41:6216–6221

Hernandez EA, Posada B, Irizarry R, Castro ME (2005) Role of hydrogen bonding interactions in directing one-dimensional thiol-assisted growth of silver-based nanofibers. J Phys Chem B 109:7251–7257

Hsu JC, Lio CH, Wei YL (2011) Nitrate removal by synthetic nanoscale zerovalent iron in aqueous recirculated reactor. Sustain Environ Res 21(6):353–359

Hwang YH, Kim DG, Shin HS (2011) Mechanism study of nitrate reduction by nano zero valent iron. J Hazard Mater 185:1513–1521

Ichiyanagi Y, Kimishima Y (2002) Structural, magnetic and thermal characterizations of Fe_2O_3 nanoparticle systems. J Therm Anal Calorim 69:919–923

Irene M (1996) Characteristics and treatment of leachates from domestic landfills. Environ Int 22(4):433–442

Jayarathne L, Ng WJ, Bandara A, Vitanage M, Dissanayake CB, Weerasooriya R (2012) Fabrication of succinic acid-γ-Fe_2O_3 nano core–shells. Colloids Surf A 403:96–102

Jun D, Yongsheng Z, Weihong Z, Mei H (2009) Laboratory study on sequenced permeable reactive barrier remediation for landfill leachate-contaminated groundwater. J Hazard Mater 161:224–230. doi:10.1016/j.jhazmat.2008.03.086

Kale SS, Kadam A, Kumar S, Pawar NJ (2010) Evaluating pollution potential of leachate from landfill site, from the Pune metropolitan city and its impact on shallow basaltic aquifers. Environ Monit Assess 162:327–346. doi:10.1007/s10661-009-0799-7

Kanel SR, Greneche J, Choi H (2006) Arsenic(V) removal from groundwater using nano scale zero-valent iron as a colloidal Reactive barrier material. Environ Sci Technol 40:2045–2050

Kanel SR, Goswami RR, Clement TP, Barnett MO, Zhao D (2008) Two dimensional transport characteristics of surface stabilized zero-valent iron nanoparticles in porous media. Environ Sci Technol 42:896–900

Karlsson MNA, Deppert K, Wacaser BA, Karlsson LS, Malm JO (2005) Size-controlled nanoparticles by thermal cracking of iron pentacarbonyl. Appl Phys A 80:1579–1583. doi:10.1007/s00339-004-2987-1

Knittle E, Phillips W, Williams Q (2001) An infrared and raman spectroscopic study of gypsum at high pressure. Phys Chem Miner 28:630–640

Krauskopf KB, Bird DK (1995) Introduction to geochemistry, 3rd edn. McGraw-Hill, New York

Kuhn LT, Bojesen A, Timmermann L, Nielsen MM, Mørup S (2002) Structural and magnetic properties of core–shell iron–iron oxide nanoparticles. J Phys Condens Matter 14:13551–13567

Lai P, Zhao HZ, Wang C, Ni JR (2007) Advanced treatment of coking wastewater by coagulation and zero valent irn process. J Hazard Mater 147:232–239

Lee M, Park K, Chung C (2000) Diffuse reflectance infrared Fourier transform spectroscopic (DRIFTS) study of self-assembled monolayers of 4-mercaptobenzoic acid on Ag powder. Bull Korean Chem Soc 21(5):532–534

Li X-q, Zhang W-x (2007) Sequestration of meta cations with zerovalent iron nanoparticles—a study with high resolution X-ray photoelectron spectroscopy (HR-XPS). J Phys Chem C 111:6939–6946

Li X, Elliott DW, Zhang W (2006) Zero-valent iron nanoparticles for abatement of environmental pollutants: materials and engineering aspects. CRC CR Rev Sol State 31:111–122. doi:10.1080/10408430601057611

Lin Y, Lin M, Liang C (2009) Characteristics and transport properties of two modified zero valent iron. Proceedings of the international conference on chemical biological and environment engineering

McIntrye NS, Zetaruk DG (1977) X-ray photoelectron spectroscopy studies of iron oxides. Anal Chem 49:1521–1529

Metcalf E (1991) Wastewater engineering: treatment, disposal and reuse, 3rd edn. McGraw Hill, New York

Mino T, Loosdrecht MCMV, Heijnen JJ (1998) Microbiology and Biochemistry of the enhanced biological phosphate removal process. War Res 32(11):3193–3207

Mor S, Ravindra K, Dahiya RP, Chandra A (2006) Leachate characterization and assessment of groundwater pollution near municipal solid waste landfill site. Environ Monit Assess 118:435–456. doi:10.1007/s10661-006-1505-7

Mullet M, Guillemin Y, Ruby C (2008) Oxidation and deprotination of sythetic FeII–FeIII(oxy)hydroxycarbonate Green Rust: an X-ray photoelectron study. J Solid State Chem 181:81–89

Nesbitt HW, Bancroft GM, Davidson R, McIntyre NS, Pratt AR (2004) Minimum XPS core-level line widths of insulators, including silicate minerals. Am Mineral 89:878–882

Parkhurst DL, Appelo CAJ (1999) User's guide to PHREEQC (version 2)—a computer program for speciation, batch-reaction, one-dimensional transport, and inverse geochemical calculations Water-Resources Investigations Report 99–4259 US Geological Survey Denver

Peter A (2001) The elements of physical chemistry, 3rd edn. Oxford University Press, New York

Pretsch E, Clerc T, Seibl J, Simon W (1989) Tables of spectral data for structure determination of organic compounds, 2nd edn. Springer-Verlag, Berlin Heideberg

Shea PJ, Machacek TA, Comfort SD (2004) Accelerated remediation of pesticide-contaminated soil with zerovalent iron. Environ Pollut 132:183–188. doi:10.1016/j.cnvpol.200405.003

Stuart B (1996) Modern infrared spectroscopy. Wiley, England. ISBN 0471959170

Sun B, Zhao FJ, Lombi E, McGrath SP (2001) Leaching of heavy metals from contaminated soil using EDTA. Environ Pollut 113: 111–120

Sun Y-p, X-q L, Cao J, W-x Z, Wang HP (2006) Characterisation of zero-valent iron nanoparticles. Adv Colloid Interface Sci 120:47–56

Tomonari M, Sadohara H, Yonezawa T, Mori K, Yamashita H (2007) Synthesis of nano-sized Ag metal particles protected by adsorbed 3-mercapto-propionic acid. J Ceram Process Res 8(3):195–198

Trankler J, Visvanathan C, Kuruparan P, Tubtimthai O (2005) Influence of tropical seasonal variations on landfill leachate characteristics—results from lysimeter studies. Waste Manag 25(10):1013–1020. doi:10.1016/j.wasman.2005.05.004

Uegami M, Kawano J, Okita T, Fujii Y, Okinaka K, Kakuya K, Yatagai S (2003) Iron particles for purifyng contiminated soil or groundwater. Process for producing the iron particles, purifying agent comprising the iron particles, process for producing the purifying agent and method of purifying contaminate soil or groundwater U.S Patent 20030217974A1

Wang CB, Zhang WX (1997) Synthesizing nanoscale iron particles for rapid and complete dechlorination of TCE and PCBs. Environ Sci Technol 31(7):2154–2156

Wang KS, Lin CL, Wei MC, Hsui WL, Li HC, Chang CH, Fang YT, Chang SH (2010) Effect of dissolved oxygen on dye removal by zero valent iron. J Hazard Mater 182:886–895

Xu X, Zhao D (2007) Reductive immobilization of chromate in water and soil using stabilized iron nanoparticulates. War Res 41:2101–2108

Xu Y, Miladinov V, Hanna MA (2004) Synthesis and characterization of starch acetates with high substitution. Cereal Chem 81(6):735–740